Advances in Materials Research, *Vol. 13, No. 6 (2024) 487-506*
https://doi.org/10.12989/amr.2024.13.6.487

Orientation of fiber effect on stiffness degradation in hygrothermal aged and cracked composite laminates - desorption case

Mohamed Khodjet-kesba*[1], B. Boukert[1a], A. Benkhedda[1b] and E.A. Adda bedia[2c]

[1]*Aeronautical Sciences Laboratory, Aeronautics and space studies Institute, University of Blida1, Algeria*
[2]*Materials and Hydrology Laboratory, University of Sidi Bel Abbes, Algeria*

(*Received August 23487, 2023, Revised July 19, 2024, Accepted September 20, 2024*)

Abstract. A modified Shear-lag model and variational approach were used to predict the effect of the crack density on stiffness degradation for $[\beta_m/\theta_n]_s$ composite laminates under different environmental conditions by the temperature variation and transient moisture concentration distribution in desorption case. Good agreement is obtained between the prediction models and experimental data published by Joffe and Katerelos, one reason for disagreement is damage in 40° layer and interface delamination that are not included in analysis. When the uncracked angle-ply laminate is submitted to hygrothermal conditions, the transient non-uniform moisture concentration distribution gives rise to relative reduction of the longitudinal Young's modulus. The results indicate that plies with a high orientation angle are more significantly affected by hygrothermal conditions, leading to greater degradation of mechanical properties, particularly Young's modulus. Furthermore, for cracked laminate $[\beta/90_3]_s$ with transverse crack, the total stiffness is significantly reduced as transverse crack density and fiber angle orientation increase in the outer layer, coupled with rising temperature and moisture concentration. However, the relative stiffness for $[0/\theta_3]_s$ cracked laminate, decreases more substantially when the fiber angle orientation is less than 90° in cracked plies with transverse crack and under various environmental conditions. The present study underscores the significance of comprehending the degradation of stiffness in the aged and cracked laminates, particularly with different fiber orientation angle.

Keywords: desorption; hygrothermal effect; stiffness reduction; transverse cracking; Tsai model

1. Introduction

For multidirectional composite laminates, the first damage that appears under uniaxial load is matrix cracking in off-axis plies (Hashin 1985). In most cases, the studies are limited to the analysis of cross-ply lay-ups (Berthelot *et al*. 1997, Hashin 1985). General off-axis laminate behaves differently with cracks development sense in more stable manner with applied load and time (Rezoug *et al*. 2011). Cracks density depends on the laminate stacking sequence, ply thicknesses, layer orientations with respect to the load direction, mechanical properties and fracture toughness in

*Corresponding author, Ph.D., E-mail: mkhojet@gmail.com
[a] Ph.D., E-mail: bilanosky@hotmail.fr
[b] Ph.D., E-mail: benkhedda90@hotmail.com
[c] Professor, E-mail: addabed@yahoo.com

http://www.techno-press.org/?journal=amr&subpage=5 ISSN: 2234-0912 (Print), 2234-179X (Online)

particular, loading direction, moisture and temperature variation (Khodjet *et al*. 2016, 2018, 2019, 2021).

Boukert *et al*. (2024) studied the prediction of stiffness degradation in composite laminate with transverse cracking and delamination under hygrothermal conditions in desorption case employing a modified shear lag model ,incorporating parabolic analysis and progressive shear to forecast the impact of transverse cracks and delamination on the stiffness degradation of transiently hygrothermal aged composite laminates, good agreement was obtained with experimental data, Tsai model was used for the introduction of aging progression at fiber and matrix scales.

Wang *et al*. (2023b) developed a new modeling approach to predict the durability of glass fiber reinforced polymer (GFRP) composites, addressing the limitations of traditional experimental methods that are time-consuming and labor-intensive. They simulated the diffusion-degradation process of GFRP in moist environments using a finite element model with a hexagonal fiber arrangement. This model, combined with test results on fiber degradation in wet conditions, enabled the calculation of time-dependent tensile strength degradation. A refined model accounted for defects such as matrix cracking and fiber/matrix debonding. The proposed framework applies to any member size and geometry, providing a quick method for predicting the long-term tensile.

Aceti *et al*. (2023) investigated strategies to mitigate the effects of hygrothermal aging, aiming to extend service life and enhance safety margins. The study emphasized the critical role of material and manufacturing process selection in addressing hygrothermal aging. It explored the impact of surface and fiber treatments on moisture uptake and reviewed techniques for moisture detection and removal. Early detection and removal of moisture were highlighted as key to preventing irreversible mechanical property loss.

Hussnain *et al*. (2023) reviewed the effects of hygrothermal aging on the mechanical performance of fiber-reinforced polymer composites (FRPCs), identifying gaps in the existing literature and suggesting future research directions. They discussed various damage prediction models for hygrothermal environments. These composites are exposed to high temperatures and moisture during service, leading to water absorption, which causes anisotropic expansion and residual stresses, thereby reducing durability. The study highlighted that the impact of hygrothermal aging varies based on factors such as fabric architecture, polymer matrix, environmental conditions, and manufacturing-induced defects.

Wang *et al*. (2023a) investigated the hygrothermal aging of carbon fiber reinforced polymer (CFRP) using accelerated aging tests over 28 days in an 80°C/95% RH environment. They examined the effects of different test temperatures on CFRP's failure strength. The study observed changes in fracture failure morphology, glass transition temperature (Tg), and the absorbance of certain functional groups post-aging. Results showed that the interlaminar failure strength of CFRP decreased in a cubic polynomial manner with aging time, being significantly lower at high temperatures compared to room temperature.

Yas *et al*. (2023) conducted a study on the buckling analysis and optimization of trapezoidal composite plates under hygrothermal conditions. They derived stability equations using first-order shear deformation theory (FSDT) and the energy method, employing the generalized differential quadrature (GDQ) method to determine critical buckling temperature and moisture content. The study examined the effects of temperature, humidity, lay-up, boundary conditions, and geometry on the stability of trapezoidal composite plates. Numerical results highlighted the significant impact of high-temperature and high-humidity environments on the buckling response of these structures.

Tamraket *et al*. (2023) examined the recyclability of nine types of composites, including those with natural and mineral fillers in polypropylene and nylon matrices, using injection moulding and

mechanical grinding. They found no significant degradation in the mechanical properties of natural fiber composites after recycling or water absorption tests. However, glass fiber composites exhibited up to a 45% decrease in tensile strength and a 40% decrease in modulus after five recycling cycles. Only glass fiber reinforced nylon composites were significantly affected by hygrothermal conditioning. At saturation, the water absorption for nylon composites reached 7.7% by weight after 45 days of immersion, which substantially impacted their mechanical properties.

Gholami *et al*. (2022a) investigated the impact of hygrothermal aging on fiber-reinforced composite materials using a multiscale finite element analysis. They examined the material's diffusivity and its spatial variation. Fick's equation was solved numerically using the finite-difference approach, considering different temperature and humidity conditions at the material boundaries. The study analysed the degradation of elastic properties, changes in thermal coefficients and moisture expansion, and the effect of the glass transition temperature on hygrothermal aging.

Gholami *et al*. (2022b) developed a coupled hygro-thermo-mechanical multiscale-APFEA (HTM-multiscale-APFEA) algorithm to accurately predict the mechanical and failure behavior of thick fiber-reinforced laminated composites under hygrothermal conditions. The Fourier and Fick's equations were simultaneously solved using a fully-coupled temperature-moisture concentration (FCTM). The study considered the impact of temperature and moisture conditions on stiffness, strength, coefficients of hygrothermal expansions (CHEs), and fracture toughness of the matrix. The HTM-multiscale-APFEA algorithm's results were validated against experimental data, analytical high-order theories, and reliable numerical analyses, the algorithm was used to analyse the failure of composite laminates under combined hygrothermal conditions and mechanical loading (bending), with results compared to experimental data. Findings indicated that in severe hygrothermal conditions at material boundaries, the composite material's transverse tensile strength, shear strength, and transverse Young's modulus degraded by approximately 72%, 13%, and 40%, respectively. The normal stiffness and strength of the cohesive/adhesive material at outer layers declined by about 73% and 47%, respectively.

Xian *et al*. (2022a) developed two types of carbon/glass fiber hybrid plates: the random hybrid (RH) and core-shell hybrid (CH) modes. They subjected these plates to sustained bending loads and water immersion for up to 360 days to investigate the influence of fiber hybrid mode and bending load on mechanical properties. Results revealed that the random hybrid mode effectively synergized carbon and glass fibers, reducing incongruous bearing behavior and stress concentration at the fiber/resin interface, thereby improving mechanical properties. Higher bending loads accelerated microcrack formation, increasing water molecule penetration, resin hydrolysis, and fiber/resin interface debonding. Tensile and flexural strength retention after five years of service ranged from 30-40% and 50-60%, respectively, offering durability guidelines for engineering applications based on fiber hybrid design.

Xian *et al*. (2022b) examined the long-term prestress loss in anchorage systems and the evolution of mechanical properties, they used a wedge-extrusion bond anchorage system to ensure reliable load-bearing capacity. A novel prestressed tension device was introduced to facilitate combined exposure to elevated temperatures (20°C, 60°C, and −20 to 30°C), distilled water, and sustained loading (20%, 40%, and 60%). The study assessed the mechanical and thermal properties of the CFRP plate under these conditions to understand its long-term behavior, tensile tests of the anchorage system revealed that the failure modes under static and cyclic loads involved CFRP bursting, with no debonding occurring in the anchor. Exposure to higher temperatures and prestress levels led to an additional degradation rate in tensile strength of 5% to 10%. The lowest strength retention of the CFRP plate was observed after 90 days of freeze-thaw exposure. Long-term life

predictions indicated that the residual tensile strength retention of CFRP plates would remain above 50% at the maximum prestress level (60%) over a service life of 30 years in civil engineering structures.

Guo *et al*. (2022) focused on the hygrothermal resistance of pultruded fiber reinforced polymer (FRP) composites. The study experimentally investigated the hygrothermal properties of pultruded carbon, glass, and carbon/glass hybrid fiber reinforced polymer (CFRP, GFRP, C/GFRP) composite plates by immersing them in deionized water at 40°C, 60°C, and 80°C for up to 135 days. The evaluation included water absorption, thermal properties, mechanical properties, and microstructure analysis to understand the long-term hygrothermal evolution. The results showed that the water absorption response of the three types of composite plates followed an initial Fickian diffusion response, followed by long-term deterioration. Immersion in deionized water led to significant degradation in thermal and mechanical properties: up to 29.5% for short beam shear strength (SBSS) of C/GFRP, 25.8% for three-point bending strength (TPBS) of GFRP, and 43.1% for glass transition temperature (Tg) of C/GFRP. Using the Arrhenius acceleration theory, the long-term life prediction showed that SBSS stabilized at 87.90% for CFRP, 76.64% for GFRP, and 72.43% for C/GFRP.

Khodjet *et al*. (2021) investigated the influence of linear and nonlinear temperature and moisture concentration distributions on the stress behavior of metal/ceramic sandwich plates with transverse cracks. The proposed model assumes an interlaminar adhesive layer between the two layers.

Khodjet *et al*. (2019) studied the hygrothermal effect on the moisture absorption in composite laminates with transverse cracks and delamination, the composite laminate is subjected to hygrothermal and mechanical loads with a transverse matrix cracking, the main idea was to predict the effect of transverse cracksband delamination on the stiffness degradation under moisture absorption for a glass-fiber/epoxy laminates with tranverse cracks only, and transverse crack plus delamination.

Khodjet *et al*. (2018) treated the issue of matrix cracking in composite laminates subjected to flexural loads under transient hygrothermal conditions. The study focused on symmetric cross-ply $[0/90]_{2s}$ laminates, utilizing a modified shear-lag model. The laminates were exposed to hygrothermal aging and moisture absorption phenomena, analyzing the resulting effects on matrix cracking behavior.

Khodjet *et al*. (2016) predicted the Poisson ratio degradation in hygrothermally aged and cracked $[0_m/90_n]_s$ composite laminates. Using a modified shear-lag model (parabolic analysis and progressive shear), the study analyzed the impact of transverse cracks on the Poisson ratio degradation in transient hygrothermally aged composite laminates.

Abualnour *et al*. (2019) examined the thermo-mechanical bending behavior of antisymmetric cross-ply laminates using a new trigonometric plate theory. Mansouri *et al*. (2019) investigated the effect of hygrothermal aging on the mechanical behavior of mixed short fiber/woven composite laminates. Various physico-chemical and mechanical tests were conducted to determine the mechanical properties under hygrothermal aging effects in aggressive environments, including distilled water, saline water at different time intervals, and high temperatures.

Huang *et al*. (2019) used a variational approach to study the behavior of laminates with transverse matrix cracks, accounting for both open and closed cracks by considering compressive and shear forces. The governing equations were derived from the variational analysis based on the principle of complementary energy. Tomonaga *et al*. (2017) focused on predicting the stiffness reduction in composite plates with transverse cracks, formulating the model based on crack density. The proposed model can predict the stiffness of composite plates with transverse cracks but does not consider damage such as delamination.

Okabe *et al*. (2017a, b) predicted the propagation of transverse cracks in composite plates using the Refined Stress Field Model, which accounts for thermal residual stresses in plates containing transverse cracks. The progression of transverse cracks in cross-ply plates is evaluated based on stress and energy criteria using the Monte Carlo method. Ghayour *et al*. (2016) developed a computational constitutive model to predict matrix cracking evolution using macro and micro models implemented using finite element analysis, the proposed model is implemented in ANSYS as a subroutine for transverse crack initiation in symmetric cross ply.

Katerelos *et al*. (2015) utilized variational models to predict the reduction in shear modulus of symmetric and balanced laminates containing cracks in the 90° layer. Their model considered the nonlinear distribution of out-of-plane shear stress thickness across all layers. Hajikezemi *et al*. (2014) analysed the stiffness reduction of symmetric laminates with a uniform distribution of matrix cracks oriented in a single direction.

The finite element models employed by Joffe and Krasnikovs (2001), Akula and Garnich (2012) were used to analyze the dependence of crack opening displacement (COD) on crack density across various angle-ply configurations of $[S/90_n]_s$ laminates. Their study yielded intriguing results, which showed significant correlation with experimental data. Lundmark and Varna (2011) utilized an interaction function to determine the crack opening displacement (COD), they developed a calculation scheme aimed at predicting stiffness reduction throughout the entire range of crack densities, the degradation of thermo-elastic properties in laminates strongly hinges on the opening and sliding of intralaminar crack surfaces during loading. Vinogradov and Hashin (2010) analysed the stiffness reduction of angle-ply laminates of type $[\theta_m^{(2)}/\ \theta_n^{(1)}]_s$ containing intralaminar cracks in the middle laminate using the principle of minimum complementary energy, an optimal admissible stress field was derived that satisfied equilibrium, boundary and traction continuity conditions, a theoretical predictions of stiffness reduction due to damage are based on the Equivalent Constraint Model (ECM), which takes into account concurrent matrix cracking in all plies of laminate was developed by Katerelos *et al*. (2008) for unbalanced symmetric $[0°/45°]_s$ glass/epoxy laminate loaded statically in tension.

In polymer composite materials, the matrix is highly susceptible to changes in moisture and temperature. Elevated levels of both factors lead to increased matrix degradation, consequently reducing the mechanical properties of composite laminates (Shen and Springer 1981, Tounsi *et al*., 2006). Tounsi and Amara (2005) investigated the hygrothermal effects on cross-ply composite laminates, focusing on the relative longitudinal Young's modulus. They conducted theoretical analyses that explicitly accounted for the temperature and moisture-induced decreases in mechanical properties, considering parameters such as fiber and matrix properties, as well as fiber volume fraction. Their findings underscored the significant impact of hygrothermal conditions on the reduction of the relative longitudinal Young's modulus, particularly at high crack densities.

After conducting an extensive literature review on hygrothermal effects and cracking in composite materials, recent studies have primarily focused on experimental aspects related to durability, mechanical performance degradation, and material damage across various fiber types and matrices. Other research has taken a theoretical approach, simulating diverse mechanical loads and boundary conditions for hygrothermal analysis. Our theoretical study delves into the behavior of composite laminates under fluctuating hygrothermal conditions, taking into account aging caused by variations in temperature and humidity. We also consider the specific damage mechanism of cracking. Integrating all these factors, our study simulates and examines how the material responds to these complex interactions.

In this paper, the modified shear-lag model and variational approach were employed to predict the impact of transverse cracks on the stiffness degradation of transient hygrothermal-aged angle-

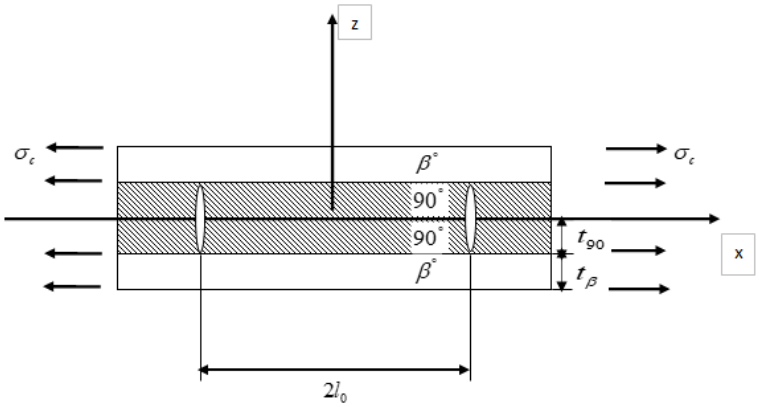

Fig. 1 Transverse cracked angle-ply $[\beta_m/90]_s$ laminate and geometric model

ply $[\beta_m/\theta_n]_s$ composite laminates. The results obtained were compared favorably with experimental data (Joffe *et al*. 2001, Katerelos *et al*. 2008) for various angle-ply laminates, albeit without considering the hygrothermal effect initially. On the other hand, the angle-ply laminate is initially exposed to hygrothermal aging due to transient and non-uniform moisture concentration distribution for desorption case. The findings demonstrate that stiffness degradation is influenced by fiber angle orientation, crack density, and the transient hygrothermal conditions during desorption.

2. Theoretical analysis

2.1 Shear-lag model

In the first case, we examine a symmetric angle-ply $[\beta_m/90]_s$ laminate under uniaxial loading conditions. It is assumed that the 90° ply has developed continuous intralaminar cracks oriented in the fiber direction, extending from edge to edge along the z-direction. The angle-ply laminate is defined by parameters: $2.t_{90}$ as the width of the 90° ply, t_β as the width of the β° ply, and a crack spacing of $2.l_0$ (refer to Fig. 1).

Where $\overline{\rho} = \frac{1}{2\cdot\overline{l_0}}; \left(\overline{l_0} = \frac{l_0}{t_{90}}\right)$ is the normalized crack density for angle-ply matrix cracks.

In the second case, matrix cracks are assumed to span theentire width and thickness of the θ°-layer throughout. A schematic of an unbalanced symmetric $[0/\theta]_s$ composite laminate with off-axis plies is shown in Fig. 2.

Where $\overline{\rho} = \frac{1}{2\cdot\overline{l_0}\cdot sin(\theta)}; \left(\overline{l_0} = \frac{l_0}{t_{90}}\right)$ is the normalized crack density for off-axis ply matrix cracks.

Strain- stress equations are given in the following form:

a) In the β° layer:

$$\begin{Bmatrix} \varepsilon_x^\beta \\ \varepsilon_y^\beta \\ \varepsilon_z^\beta \end{Bmatrix} = \begin{bmatrix} S_{xx}^\beta S_{xy}^\beta S_{xz}^\beta \\ S_{xy}^\beta S_{yy}^\beta S_{yz}^\beta \\ S_{xz}^\beta S_{yz}^\beta S_{zz}^\beta \end{bmatrix} \begin{Bmatrix} \sigma_x^\beta \\ \sigma_y^\beta \\ \sigma_z^\beta \end{Bmatrix} \quad (1)$$

b) In the θ° layer:

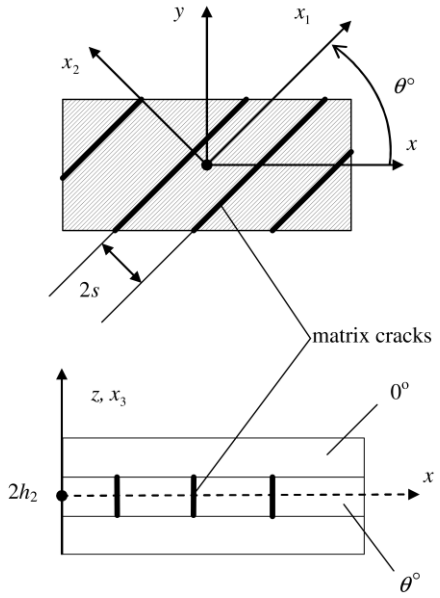

Fig. 2 Front and edge views of a $[0/\theta]_s$ laminate with off-axis ply matrix cracks (Katerelos *et al*. 2008)

$$\begin{Bmatrix} \varepsilon_x^\theta \\ \varepsilon_y^\theta \\ \varepsilon_z^\theta \end{Bmatrix} = \begin{bmatrix} S_{xx}^\theta S_{xy}^\theta S_{xz}^\theta \\ S_{xy}^\theta S_{yy}^\theta S_{yz}^\theta \\ S_{xz}^\theta S_{yz}^\theta S_{zz}^\theta \end{bmatrix} \begin{Bmatrix} \sigma_x^\theta \\ \sigma_y^\theta \\ \sigma_z^\theta \end{Bmatrix} \tag{2}$$

where S_{ij} is the compliance matrix for angle-ply laminate.

We obtain the modified expression of the longitudinal Young's modulus of the angle-ply laminate due to transverse cracks:

$$\frac{E_x}{E_{x0}} = \frac{1}{1 + \frac{E_\theta t_\theta}{E_\beta t_\beta} \frac{(1 - \upsilon_{12}\upsilon_{xy}^0)}{(1 - \upsilon_{12}\upsilon_{21})} \frac{1}{2a} R(a) \left(1 + \upsilon_{xy}^\beta \frac{(s_{xy}^\beta t_{90} + s_{12} t_\beta)}{(s_{yy}^\beta t_{90} + s_{11} t_\beta)}\right)} \tag{3}$$

The model developed by Berthelot (1997) is used, this latter is modified by introducing the stress perturbation function:

$$R(a) = \int_{-a}^{+a} \frac{cosh(\xi \overline{x})}{cosh(\xi a)} d\overline{x} = \frac{2}{\xi} tanh(\xi a) \tag{4}$$

where, ξ is the shear-lag parameter:

$$\xi^2 = \overline{G} \frac{t_\theta (t_\theta E_\theta + t_\beta E_\beta)}{t_\beta E_\theta E_\beta} \tag{5}$$

The coefficient $\overline{G}$ depends on used assumptions about the longitudinal displacement and shear stress distribution:

a) In case of parabolic variation of longitudinal displacement assumption displacement in both β° and θ° layers, the coefficient $\overline{G}$ is done by (Adda bedia *et al*. 2008):

• The first case assumes that the longitudinal displacement is parabolic in θ° layer thickness:

$$u_\theta(x,z) = \overline{u_\theta}(x) + \left(z^2 - \frac{t_\theta^2}{3}\right) A_\theta(x) \tag{6}$$

The variation of the longitudinal displacement is to be determined in β° layers thickness:

$$u_\beta(x,z) = \overline{u_\beta}(x) + f(z) A_\beta(x) \tag{7}$$

• The second case assumes that the shear stresses, which are similar in θ° and β° layers, can be obtained by assuming that the transverse displacement is independent of the longitudinal coordinate:

$$\sigma_{xz}^i = G_{xz}^i \gamma_{xz}^i \tag{8}$$

$$\gamma_{xz}^i = \frac{\partial u_i}{\partial z} + \frac{\partial w_i}{\partial x} \approx \frac{\partial u_i}{\partial z} \qquad i = \theta°, \beta° \tag{9}$$

The coefficient $\overline{G}$ is done by (Adda bedia *et al*. 2008):

$$\overline{G} = \frac{3G}{t_{90}} \tag{10}$$

The shear modulus G of the elementary cell:

$$G = \frac{G_{xz}^\theta}{1 - 3\frac{G_{xz}^\theta}{G_{xz}^\beta}\frac{f(t_\theta)}{t_\theta f'(t_\theta)}} \tag{11}$$

By replacing the function $f(z) = z^2 - 2\left(t_\beta + t_\theta\right)z + \frac{2}{3}t_\beta^2 + 2t_\beta t_\theta + t_\theta^2$ in (11), the shear modulus for parabolic assumption will be:

$$G = \frac{G_{xz}^\theta}{1 + \alpha\frac{G_{xz}^\theta}{G_{xz}^\beta}} \tag{12}$$

b) When the variation of the longitudinal displacement is supposed progressive in 0^0 layer:

We use the function $f(z) = \frac{sinh\,\alpha\eta_t}{\alpha\eta_t} - cosh\,\eta_t\left(1 + \alpha - \frac{z}{t_\theta}\right)$ in (11), the shear modulus for progressive shear assumption will be:

$$G = \frac{G_{xz}^\theta}{1 + 3\alpha\frac{\alpha\eta_t(tanh\,\alpha\,\eta_t)^{-1} - 1}{\alpha\eta_t^2}\frac{G_{xz}^\theta}{G_{xz}^\beta}} \tag{13}$$

2.2 Variational approach

The variational approach assumes that the axial stress distribution across the layer width is assumed in θ° and β° layers (Hashin 1985, 1986). This assumption generates linear distributions for shear stresses and parabolic in z-axis direction. Expressions for x-axis stress components are the following:

$$\sigma_{xx}^\theta = \sigma_\theta(1 - \varphi_1(x)) \tag{14}$$

$$\sigma_{xx}^\beta = \sigma_\beta(1 - \varphi_2(x)) \tag{15}$$

where σ_θ is the stress in θ° layer before cracking, calculated by laminated plate theory for undamaged angle-ply. $\frac{\sigma_\theta}{\sigma_c} = \frac{E_\theta}{E_x^0}$

σ_β is the stress in β ° layer before cracking, calculated by laminated plate theory for undamaged angle-ply. $\frac{\sigma_\beta}{\sigma_c} = \frac{E_\beta}{E_x^0}$

φ_1, φ_2 are unknown functions.

Next, we denote

$$\varphi_1(x) = \varphi(x) \tag{16}$$

and express $\varphi_2(x)$ in term of $\varphi(x)$ due to equilibrium condition in x direction:

$$\sigma_\beta t_\beta \varphi_1(x) + \sigma_\theta t_\theta \varphi_2(x) = 0 \tag{17}$$

Final expression for complementary energy will be:

$$u_c^{'} = \frac{1}{2}\sigma_\theta^2 t_\theta^2 \int_{-a}^{+a} \left(C_{00}\varphi^2 + C_{02}\varphi + C_{22}\left(\frac{d^2\varphi}{d\xi^2}\right)^2 + C_{11}\left(\frac{d\varphi}{d\xi}\right)^2 \right) d\xi \tag{18}$$

where:

$$C_{00} = \frac{1}{E_\theta} + \frac{1}{\alpha E_\beta} \tag{19}$$

$$C_{02} = \frac{\upsilon_\theta}{E_\theta}\left(\alpha + \frac{2}{3}\right) - \frac{\alpha \upsilon_\beta}{3E_\beta} \tag{20}$$

$$C_{22} = \frac{1}{60E_\theta}(\alpha + 1)(3\alpha^2 + 12\alpha + 8) \tag{21}$$

$$C_{11} = \frac{1}{3}\left(\frac{1}{G_\theta} + \frac{\alpha}{G_\beta}\right) \tag{22}$$

$$\alpha = \frac{t_\beta}{t_\theta} \tag{23}$$

The function φ which minimizes the complementary energy $u_c^{'}$ is the fourth order differential equation of Euler-Lagrange:

$$\frac{d^4\phi}{d\xi^4} + p\frac{d\phi^2}{d\xi^2} + q\phi = 0 \tag{24}$$

$$p = \frac{C_{02} - C_{11}}{C_{22}}, \qquad q = \frac{C_{00}}{C_{22}} \tag{25}$$

Provided that $4q > p^2$. Consequently, the solutions are :

$$\varphi = A_1 ch\alpha\xi \cos\beta\,\xi + A_2 sh\alpha\xi \sin\beta\,\xi \tag{26}$$

with

$$A_1 = \frac{2(\alpha \cdot cha a \cdot \sin\beta\, a + \beta \cdot sha a \cdot \cos\beta\, a)}{\alpha \cdot \sin 2\,\beta a + \beta \cdot sh2\alpha a} \tag{27}$$

$$A_2 = \frac{2(\beta \cdot cha a \cdot \sin \beta\, a + \alpha \cdot sha a \cdot \cos \beta\, a)}{\alpha \cdot \sin 2\,\beta a + \beta \cdot sh2\alpha a} \tag{28}$$

and

$$\alpha = q^{\frac{1}{4}} \cos\frac{\theta}{2};\ \beta = q^{\frac{1}{4}} \sin\frac{\theta}{2};\ \theta = arctg\sqrt{\frac{4q}{p^2} - 1} \tag{29}$$

The reduced stiffness E_x can be expressed in the following form (Hashin 1986):

$$\frac{E_x}{E_{x0}} = \frac{1}{1 + \frac{E_\theta}{E_\beta}\frac{t_\theta}{t_\beta}\frac{1}{\overline{l_0}} g(\overline{l_0})} \tag{30}$$

where $g(\overline{l_0})$ is expressed as:

$$g(\overline{l_0}) = \frac{2\delta\beta}{\delta^2 + \beta^2} \frac{cosh(2\delta\overline{l_0}) - cos(2\beta\overline{l_0})}{\delta \sin(2\beta\overline{l_0}) + \beta \sinh(2\delta\overline{l_0})} \tag{31}$$

3. Results and discussion

A computer code based on the preceding equations was developed to calculate the stiffness degradation, considering both with and without the hygrothermal effect.

3.1 Reduction of longitudinal Young's modulus for $[\beta_m/90_n]_s$

In this section we will validate the results of our program without considering the hygrothermal effect on material properties. The results will be compared with experimental data for a glass/epoxy laminate (Joffe *et al*. 2001). The material properties of the selected composite and their geometrical characteristics are summarized in Table 1.

The longitudinal Young's modulus degradation due to transverse cracks for glass/epoxy composite with different angle-ply laminates are shown in Figs. 3-6. These figures predict the stiffness reduction by shear-lag model and variational approach compared with experimental data published by Joffe (2001). A good agreement is obtained between shear-lag model and experimental data when fiber orientation of the outer layers is less than 40° (Figs. 3-5). When we have a $[\pm 40/90_4]_s$ glass/epoxy laminate (Fig. 6), only the variational model seems in good agreement with experimental data to predict longitudinal Young's modulus degradation. One reason for disagreement is damage in 40° layer and interface delamination that are not included in analysis. Delamination leads to larger crack opening and results in larger stiffness reduction. Variational approach is more accurate to predict stiffness degradation on angle-ply laminates containing delamination due to transverse cracks tips.

Table 1 Material properties of glass/epoxy laminate (Joffe *et al*. 2001).

Proprieties/ Material	E_L (GPa)	E_T (GPa)	G_{LT} (GPa)	$G_{TT'}$ (GPa)	υ_{LT}	$\upsilon_{TT'}$	t_{90} (mm)
Glass/epoxy	44.73	12.76	5.8	4.49	0.297	0.42	0.144

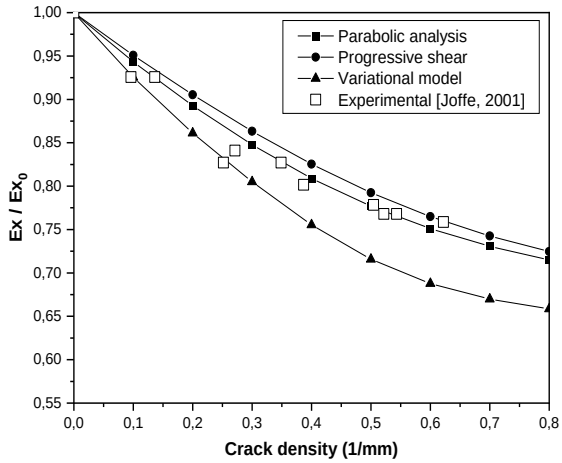

Fig. 3 Longitudinal Young's modulus degradation due to transverse cracks in a $[0_2/90_4]_s$ glass/epoxy laminate

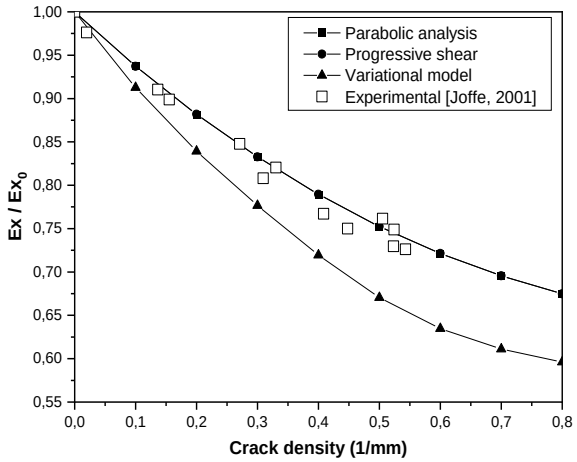

Fig. 4 Longitudinal Young's modulus degradation due to transverse cracks in a $[\pm 15/90_4]_s$ glass/epoxy laminate

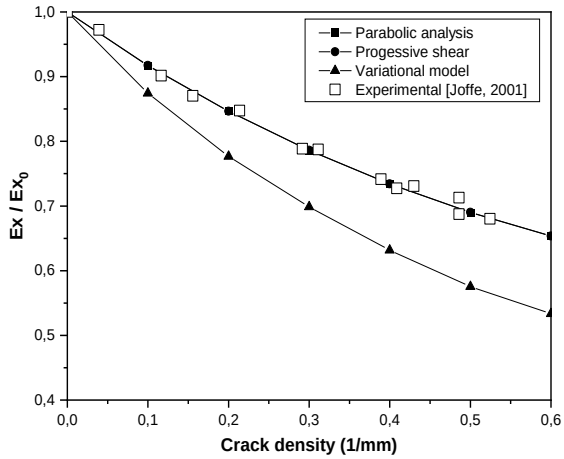

Fig. 5 Longitudinal Young's modulus degradation due to transverse cracks in a $[\pm 30/90_4]_s$ glass/epoxy laminate

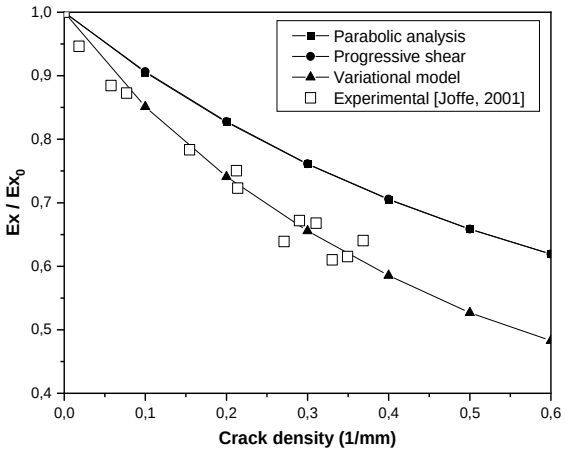

Fig. 6 Longitudinal Young's modulus degradation due to transverse cracks in a $[\pm 40/90_4]_s$ glass/epoxy laminate

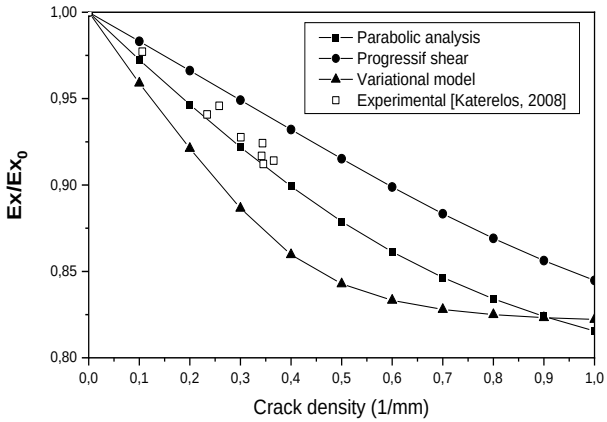

Fig. 7 Longitudinal Young's modulus degradation due to transverse cracks in a $[0/45]_s$ glass/epoxy laminate with t_{45}=0.61mm

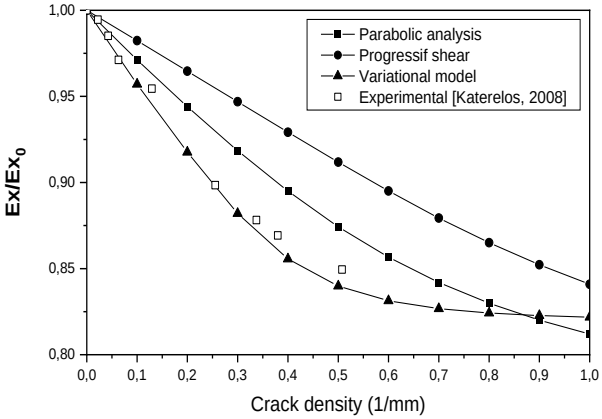

Fig. 8 Longitudinal Young's modulus degradation due to transverse cracks in a $[0/45]_s$ glass/epoxy laminate with t_{45}=0.64mm

Table 2 Mechanical properties of glass/epoxy composite laminas

Layer angle	E_1 (GPa)	E_2 (GPa)	G_{12} (GPa)	υ_{12}
0° layer	43	13	4.69	0.3
90° layer	13	43	4.69	0.09
45° layer	13.36	13.36	8.76	0.42

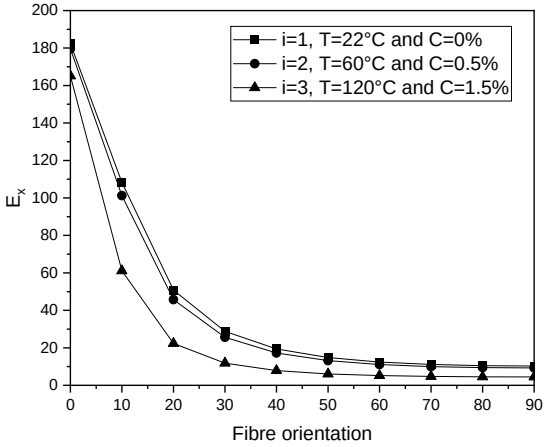

Fig. 9 Longitudinal Young's modulus degradation as a function of fiber orientation for a graphite/epoxy (T300/5208) laminate with different hygrothermal conditions

3.2 Longitudinal Young's modulus reduction for $[0_m/\theta_n]_s$

Numerical simulations are performed for glass/epoxy composite (Katerelos *et al*. 2008), material properties are shown in Table 2.

Figs. 7 and 8 show another results comparison obtained by analytical models and experimental data (Katerelos *et al*. 2008) for $[0/45]_s$ glass/epoxy laminate with two different thickness. To accommodate variation in ply thickness observed in test specimens, the model was run twice – first time assuming all layers have thickness 0.61 mm, and the second 0.64 mm; however, small variation in ply thickness has very little effect on the predicted Young's modulus value. The quantity ''crack density'' refers to the linear crack density at each loading level, which is the number of cracks per unit length. In all cases the experimental crack density has been derived by dividing the number of the fully developed cracks to the actual ''window'' length (Katerelos *et al*. 2008). The parabolic model seems always closer to experimental data compared to progressive shear and variational model (Fig. 7). On the other side, by increasing the thickness of the 45° cracked layer (Fig. 8), the variational analysis become closer to experimental data which gives an advantage to this method to represent the behavior of $[\beta_m/\theta_n]_s$ composite laminate under transverse cracking and delamination effect.

3.3 Hygrothermal conditions Influence on reduced Young's modulus

Our study focuses on stiffness reduction due to transverse ply cracking in $[\beta/\theta_3]_s$ laminate when it is initially exposed to hygothermal aging, subjected to transient and non-uniform moisture

concentration distribution during desorption. The Tsai model (Tsai 1988) will enable us to introduce aging and observe its effects on the fiber and matrix scales.

Tsai (1988) proposes an adimensional temperature T*, which is the essential parameter for hygrothermal effect evaluation in stress distribution:

$$T^* = \frac{T_g - T_{opr}}{T_g - T_{rm}} \tag{32}$$

where T_g is the glass transition temperature, T_{opr} is the operating temperature and T_{rm} is the room temperature.

We further assume that moisture suppresses the glass transition temperature T_g^0 by simple temperature shift.

$$T_g = T_g^0 - gc \tag{33}$$

The longitudinal Young's modulus degradation as a function of fiber orientation for a graphite/ epoxy (T300/5208) with different environmental conditions is shown in Fig.9. A significant degradation of the Young's modulus is observed with the increase in fiber orientation angle, reaching a maximum value of approximately 60% for an angle of 45° (see table 3). Beyond this point, the degradation stabilizes (while maintaining a high rate) when the fiber orientation angle approaches 90°. This behavior indicates that plies with a high orientation angle are more significantly affected by hygrothermal conditions, resulting in greater degradation of mechanical properties, particularly Young's modulus.

We consider a laminated plate of thickness h made of composite polymer matrix. The plate is subjected to the same dry environment on both sides. It is assumed to be infinite in both the x and y directions, with moisture varying only in the z direction. Initially, the moisture concentration C_{init} is uniform at t=0. Both sides are suddenly exposed to a zero-moisture environment (Fig. 10). The moisture concentration within the plate is governed by Fick equation (Shen and Springer 1981, Benkhedda *et al*. 2008) with diffusivity D_z.

$$\frac{\partial C}{\partial t} = D_z \frac{\partial^2 C}{\partial z^2} \tag{34}$$

With the initial conditions:

$C=C_{init}$ for $-h/2 \le z \le h/2$ and $t = 0$

$C=0$ for $z=-h/2$; $z= h/2$ and $t >0$

The initial conditions being uniform and boundary conditions are constants, the unidimensional solution of Fick equation can be expressed as (Shen and Springer 1981, Benkhedda *et al*. 2008):

$$C(z_k, t) = \left[\frac{4C_{ini}}{\prod}\sum_{n=0}^{\infty}\frac{(-1)^n}{(2n+1)}cos\left(\frac{(2n+1)\prod z_k}{h}\right)exp\left(\frac{-D_z(2n+1)^2\prod^2 t}{h^2}\right)\right] \tag{35}$$

The stiffness loss of the laminate with a known crack density is evaluated compared to the initial stiffness of the same uncracked laminate under identical environmental conditions. It is noted that the initial stiffness of the uncracked laminate varies with temperature and moisture distribution. Therefore, Eqs. (3) and (30) are modified accordingly:

$$\frac{E_{x(i)}}{E_{x0(i)}} = \frac{1}{1 + \frac{E_{\theta(i)}t_\theta}{E_{\beta(i)}t_\beta}\frac{(1-\upsilon_{12}\upsilon_{xy}^0)}{(1-\upsilon_{12}\upsilon_{21})}\frac{1}{2a}R_{(i)}(a)\left(1+\upsilon_{xy}^\beta\frac{(s_{xy}^\beta t_\theta + s_{12}t_\beta)}{(s_{yy}^\beta t_{90} + s_{11}t_\beta)}\right)} \tag{36}$$

Table 3 Relative gap related to Young's modulus for different fibre orientation and environmental conditions

Ex (GPa) Fibre orientation	i=1 (T=22°C and C=0%)	i=2 (T=60°C and C=0.5%)	i=3 (T=120°C and C=1.5%)	Relative gap $\left(\frac{i=1-i=3}{i=1}\right)$
0	182.32	179.62	165.15	9.42%
10	108.30	101.23	61.10	43.58%
20	50.80	45.73	22.34	56.01%
30	28.81	25.64	11.84	58.91%
40	19.41	17.24	7.87	59.43%
50	14.83	13.19	6.07	59.07%
60	12.42	11.09	5.18	58.30%
70	11.13	9.97	4.74	57.44%
80	10.49	9.43	4.54	56.77%
90	10.30	9.26	4.48	56.51%

Table 4 Fiber and matrix characteristics of graphite/epoxy material (T300/5208) (Tsai 1988)

E_{fx} (Gpa)	E_{fy} (Gpa)	ν_{fx}	E_m (Gpa)	ν_m	G_m (Gpa)	G_{fx} (Gpa)	V_f
259	18.69	0.25	3.4	0.35	1.26	19.69	0.7

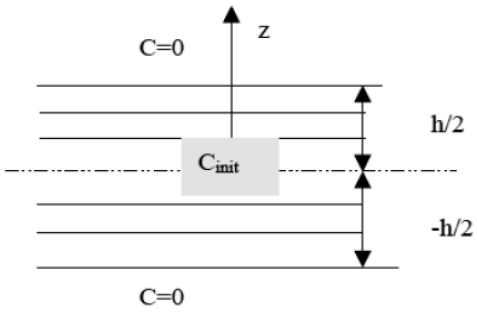

Fig. 10 Desorption phase

$$\frac{E_{x(i)}}{E^0_{x(i)}} = \frac{1}{1+\frac{E_{\theta(i)}}{E_{\beta(i)}}\frac{t_\theta}{t_\beta}\frac{1}{\overline{l_0}}g_{(i)}(\overline{l_0})} \tag{37}$$

The total stiffness reduction modulus is determined compared to the axial modulus of the uncracked laminate when it is initially exposed to environmental condition (i=1). Therefore, this total stiffness reduction takes into account the reduction due to the crack density, moisture and temperature variation.

$$\frac{E_{x(i)}}{E_{x0(1)}} = \frac{\left(\alpha E_{\beta(i)} + E_{\theta(i)}\right)}{1+\frac{E_{\theta(i)}t_\theta}{E_{\beta(i)}t_\beta}\frac{\left(1-\upsilon_{12}\upsilon^0_{xy}\right)}{(1-\upsilon_{12}\upsilon_{21})}\frac{1}{2a}R_{(i)}(a)\left(1+\upsilon^\beta_{xy(i)}\frac{(S_{12}t_\theta+S_{12}t_\beta)}{(S_{22}t_\theta+S_{11}t_\beta)}\right)\left(\alpha E_{\beta(1)}+E_{\theta(1)}\right)} \tag{38}$$

Table 5 Relative gap related to total stiffness of cracked graphite/epoxy for different fiber orientation and environmental conditions

$\frac{E_{x(i)}}{E_{x(1)}}$ Crack density	$[0/90_3]_s$				$[15/90_3]_s$			
	i=1 (T=22°C and C=0%)	i=2 (T=60°C and C=0.5%)	i=3 (T=120°C and C=1.5%)	Relative gap $\left(\frac{i=1-i=3}{i=1}\right)$	i=1 (T=22°C and C=0%)	i=2 (T=60°C and C=0.5%)	i=3 (T=120°C and C=1.5%)	Relative gap $\left(\frac{i=1-i=3}{i=1}\right)$
0	1.00	0.98	0.91	9.12%	1.00	0.92	0.70	30.48%
0.2	0.98	0.95	0.89	8.34%	0.95	0.87	0.66	28.89%
0.4	0.95	0.93	0.88	7.61%	0.90	0.83	0.63	27.47%
0.6	0.93	0.91	0.86	6.95%	0.86	0.79	0.60	26.19%
0.8	0.91	0.90	0.85	6.40%	0.83	0.76	0.58	25.10%
1	0.90	0.88	0.84	5.96%	0.80	0.74	0.56	24.21%
1.2	0.89	0.88	0.83	5.63%	0.78	0.72	0.55	23.52%
1.4	0.88	0.87	0.83	5.37%	0.77	0.70	0.54	22.98%
1.6	0.88	0.86	0.83	5.18%	0.76	0.69	0.53	22.57%
1.8	0.87	0.86	0.82	5.04%	0.75	0.69	0.52	22.25%
$\frac{E_{x(i)}}{E_{x(1)}}$ Crack density	$[30/90_3]_s$				$[40/90_3]_s$			
	i=1 (T=22°C and C=0%)	i=2 (T=60°C and C=0.5%)	i=3 (T=120°C and C=1.5%)	Relative gap $\left(\frac{i=1-i=3}{i=1}\right)$	i=1 (T=22°C and C=0%)	i=2 (T=60°C and C=0.5%)	i=3 (T=120°C and C=1.5%)	Relative gap $\left(\frac{i=1-i=3}{i=1}\right)$
0	1.00	0.90	0.66	34.10%	1.00	0.90	0.66	34.07%
0.2	0.90	0.81	0.59	30.97%	0.87	0.78	0.57	30.04%
0.4	0.82	0.73	0.53	28.36%	0.77	0.69	0.50	26.84%
0.6	0.75	0.67	0.49	26.16%	0.69	0.62	0.45	24.26%
0.8	0.69	0.62	0.45	24.35%	0.63	0.56	0.40	22.19%
1	0.65	0.58	0.42	22.90%	0.58	0.52	0.37	20.54%
1.2	0.62	0.55	0.40	21.77%	0.54	0.48	0.35	19.25%
1.4	0.59	0.53	0.38	20.89%	0.51	0.46	0.33	18.25%
1.6	0.57	0.51	0.37	20.21%	0.49	0.44	0.31	17.48%
1.8	0.56	0.50	0.36	19.68%	0.47	0.42	0.30	16.87%

The index (i) represents the considered case of environmental conditions.

The longitudinal Young's modulus degradation of a cracked laminate is represented in an angle-ply $[\beta/\theta_3]_s$ configuration, where the laminate is exposed to hygrothermal conditions with a parabolic variation of longitudinal displacement in both β° and θ° layers (transverse cracks are in θ° layers). Transient and non-uniform moisture concentration has been selected to simulate temperature and moisture effects in cracked angle-ply laminates for the desorption case. Three sets of environmental conditions are considered. Environmental case 1, Top=22°C and C=0%. Environmental case 2, Top=60°C and C=0.5%. Environmental case 3, Top=120°C and C=1%. Exposition duration for simulation is equal to t_{sat}=4222h, t_{sat} is the moisture saturation time for T300/5208. The fiber & matrix Characteristics of graphite/epoxy (T300/5208) laminate are shown in Table 4.

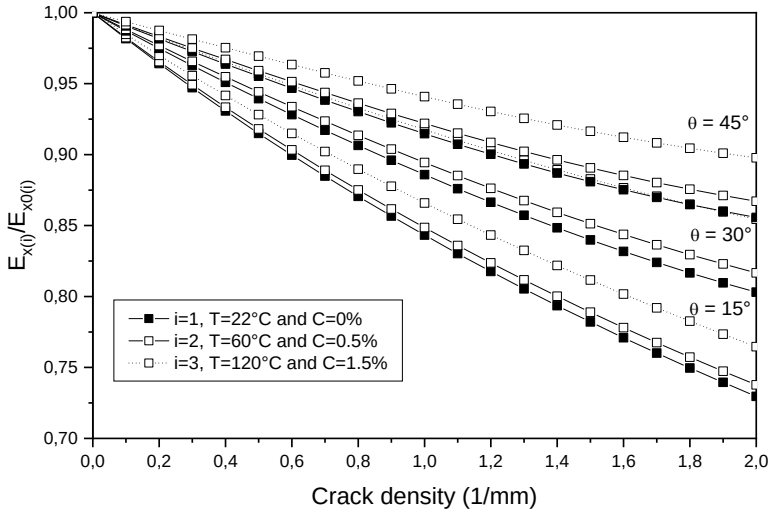

Fig. 11 Stiffness reduction as a function of crack density for a $[0/\theta_3]_s$ graphite/epoxy (T300/5208) laminate with different fibre angle θ° in the inner layer

A significant degradation in total stiffness is observed for crack densities below one, with a maximal reduction occurring when the material exhibits no cracks (see Table 5). As the crack density increases, the degradation in total stiffness becomes nearly stable, which can be attributed to the material reaching a saturation state. Furthermore, when the orientation angle of the outer layers is greater than 0°, a more significant degradation in total stiffness is observed. This suggests that cracked plies with a high orientation angle are more significantly impacted by hygrothermal conditions, leading to greater degradation of stiffness.

When the inner layer orientation is different from 90° and subjected to hygrothermal effect (Fig. 11), we note that the relative stiffness is reduced with transverse crack density and deceasing with fiber orientation θ. We observed less reduction in stiffness with the increasing of operational temperature and moisture concentration in desorption case. Finally, hygrothermal conditions have a more significant impact on the relative stiffness reduction when the cracked orientation layers are different from 90°.

4. Conclusions

The stiffness reduction was predicted using simple analytical models for the angle-ply $[\beta_m/90]_s$ and $[0/\theta_n]_s$ composite laminates configuration under uniaxial tension. The results show good agreement between prediction models and experimental data. The best fit with experimental data is shear lag model. which assumes a complete parabolic displacement distribution. On the other hand, the material properties are considered to be dependent on temperature and moisture concentration, which are given explicitly in terms of fiber and matrix properties and fiber volume ratio. The fiber orientation is an important parameter of moisture diffusion behavior. The solution methodology is general and may be applied to analyze other types of environmental condition. e.g. including hygrothermal coupling in governing equation. Based on the findings presented herein, the following conclusions can be drawn:

• The analytical model based on shear lag theory aligns well with the experimental data when the fiber orientation of the outer layers is below 40 degrees.

• When the fiber orientation angle of the outer layers is 40°, the variational model is the only one that accurately predicts the degradation of longitudinal Young's modulus in agreement with the experimental data. This increases the model's accuracy in predicting stiffness degradation on angle-ply laminates containing delamination due to transverse cracks tips.

• In the case of the uncracked angle-ply laminate, the degradation of Young's modulus under hygrothermal conditions becomes more pronounced with higher fiber orientation angles.

• The reduction in total stiffness of the cracked laminate $[\beta/90_3]_s$ becomes more pronounced with increasing fiber orientation angles of the outer layers, as well as temperatures and moisture concentrations.

References

Abualnour, M., Chikh, A., Hebali, H., Kaci, A., Tounsi, A., Bousahla, A.A. and Tounsi, A. (2019), "Thermomechanical analysis of antisymmetric laminated reinforced composite plates using a new four variable trigonometric refined plate theory", *Comput. Concr.*, **24**(6), 489-498. http://doi.org/10.12989/cac.2019.24.6.489.

Aceti, P., Carminati, L., Bettini, P. and Sala, G. (2023), "Hygrothermal ageing of composite structures. Part 2: Mitigation techniques, detection and removal", *Compos. Struct.*, **319**, 117105. https://doi.org/10.1016/j.compstruct.2023.117105.

Adda-Bedia, E.A., Bouazza, M., Tounsi, A., Benzair, A. and Maachou, M. (2008), "Prediction of stiffness degradation in hygrothermal aged $[\theta_m/90_n]_s$ composite laminates with transverse cracking", *J. Mater. Proc. Technol.*, **199**(1-3), 199-205. https://doi.org/10.1016/j.jmatprotec.2007.08.002.

Akula, V.M.K. and Garnich, M.R. (2012), "Effective ply and constituent elastic properties for cracked laminates", *Compos. Part B Eng.*, **43**(5), 2143-2151. https://doi.org/10.1016/j.compositesb.2012.02.034.

Benkhedda, A. and Tounsi, A. (2008), "Effect of temperature and humidity on transient hygrothermal stress during moisture desorption in laminated composite plates", *Compos. Struct.*, **82**(4), 629-635. https://doi.org/10.1016/j.compstruct.2007.04.013.

Berthelot, J.M. (1997), "Analysis of the transverse cracking of cross-laminates: a generalized approach", *J. Compos. Mater.*, **31**(18), 1780-1805. https://doi.org/10.1177/002199839703101801.

Boukert, B., Khodjet-Kesba, M., Benkhedda, A. and Bedia, E.A. (2024), "Prediction of stiffness degradation in composite laminate with transverse cracking and delamination under hygrothermal conditions-desorption case", *Adv. Aircr. Spacecr. Sci.*, **11**(1), 1-21. https://doi.org/10.12989/aas.2024.11.1.001

Ghayour, M., Hosseini-Toudeshky, H., Jalalvand, M. and Barbero, E.J. (2016), "Micro/macro approach for prediction of matrix cracking evolution in laminated composites", *J. Compos. Mater.*, **50**(19), 2647-2659. https://doi.org/10.1177/0021998315610179.

Gholami, M., Afrasiab, H., Baghestani, A.M. and Fathi, A. (2022a), "A novel multiscale parallel finite element method for the study of the hygrothermal aging effect on the composite materials", *Compos. Sci. Technol.*, **217**, 109120. https://doi.org/10.1016/j.compscitech.2021.109120.

Gholami, M., Afrasiab, H., Baghestani, A.M. and Fathi, A. (2022b), "Mechanical and failure analysis of thick composites under hygrothermal conditions by a novel coupled hygro-thermo-mechanical multiscale algorithm", *Compos. Sci. Technol.*, **230**(1), 109773. https://doi.org/10.1016/j.compscitech.2022.109773.

Guo, R., Xian, G., Li, F., Li, C. and Hong, B. (2022), "Hygrothermal resistance of pultruded carbon, glass and carbon/glass hybrid fiber reinforced epoxy composites", *Constr. Build. Mater.*, **315**, 125710. https://doi.org/10.1016/j.conbuildmat.2021.125710.

Hajikazemi, M. and Sadr, M.H. (2014), "Stiffness reduction of cracked general symmetric laminates using a variational approach", *Int. J. Solids Struct.*, **51**(7-8), 1483-1493.

https://doi.org/10.1016/j.ijsolstr.2013.12.040.
Hashin, Z. (1985), "Analysis of cracked laminates: a variational approach", *Mech. Mater.*, **4**(2), 121-136. https://doi.org/10.1016/0167-6636(85)90011-0.
Hashin, Z. (1986), "Analysis of stiffness reduction of cracked cross ply laminates", *Eng. Fract. Mech.*, **25**(5-6), 771-778. https://doi.org/10.1016/0013-7944(86)90040-8.
Huang, Z.Q., Yi, S.H., Chen, H.X. and He, X.Q. (2019), "Parameter analysis of damaged region for laminates with matrix defects", *J. Sandw. Struct. Mater.*, **23**(2), 580-620. https://doi.org/10.1177/1099636219842290.
Hussnain, S.M., Shah, S.Z.H., Megat-Yusoff, P.S.M. and Hussain, M.Z. (2023), "Degradation and mechanical performance of fibre-reinforced polymer composites under marine environments: A review of recent advancements", *Polym. Degrad. Stabil.*, **215**, 110452. https://doi.org/10.1016/j.polymdegradstab.2023.110452.
Joffe, R., Krasnikovs, A. and Varna, J. (2001), "COD-based simulation of transverse cracking and stiffness reduction in $[S/90n]_S$ laminates", *Compos. Sci. Technol.*, **61**(5), 637-656. https://doi.org/10.1016/S0266-3538(00)00172-X.
Katerelos, D.T.G., Kashtalyan, M., Soutis, C. and Galiotis, C. (2008), "Matrix cracking in polymeric composites laminates: Modelling and experiments", *Compos. Sci. Technol.*, **68**(12), 2310-2317. https://doi.org/10.1016/j.compscitech.2007.09.013.
Katerelos, D.T.G., Krasnikovs, A. and Varna, J. (2015), "Variational models for shear modulus of symmetric and balanced laminates with cracks in 90°-layer", *Int. J. Solids Struct.*, **71**, 169-179. https://doi.org/10.1016/j.ijsolstr.2015.06.017.
Khodjet-Kesba, M., Bedia, E.A., Benkhedda, A. and Boukert, B. (2016), "Prediction of Poisson's ratio degradation in hygrothermal aged and cracked $[\theta_m/90_n]_s$ composite laminates", *Steel Compos. Struct.*, **21**(1), 57-21. http://doi.org/10.12989/scs.2016.21.1.057.
Khodjet-Kesba, M., Benkhedda, A., Bedia, E.A. and Boukert, B. (2018), "On transverse matrix cracking in composite laminates loaded in flexure under transient hygrothermal conditions", *Struct. Eng. Mech.*, **67**(2), 165-173.https://doi.org/10.12989/sem.2018.67.2.165.
Khodjet-Kesba, M., Benkhedda, A. and Boukert, B. (2019), "Hygrothermal effect on the moisture absorption in composite laminates with transverse cracks and delamination", *Adv. Aircr. Spacecr. Sci.*, **6**(4), 315-331. https://doi.org/10.12989/aas.2019.6.4.315.
Khodjet-Kesba, M., Noureddine, E. and Benkhedda, A. (2021), "Stress distribution on the cracked sandwich plate with non-linear thermal and moisture concentration", *Nano Hybrids Compos.*, **32**(45-62), 2021. https://doi.org/10.4028/www.scientific.net/NHC.32.45.
Lundmark, P. and Varna, J. (2011), "Stiffness reduction in laminates at high intralaminar crack density: effect of crack interaction", *Int. J. Damage Mech.*, **20**(2), 279-297. https://doi.org/10.1177/1056789509351840.
Mansouri, L., Djebbar, A., Khatir, S. and Wahab, M.A. (2019), "Effect of hygrothermal aging in distilled and saline water on the mechanical behaviour of mixed short fibre/woven composites", *Compos. Struct.*, **207**, 816-825. https://doi.org/10.1016/j.compstruct.2018.09.067.
Okabe, T., Onodera, S., Kumagai, Y. and Nagumo, Y. (2017a), "Prediction for progression of transverse cracking in CFRP cross-ply laminates using Monte Carlo method", *Adv. Compos. Mater.*, **26**(5), 477-491. https://doi.org/10.1080/09243046.2017.1325076.
Okabe, T., Onodera, S., Kumagai, Y. and Nagumo, Y. (2017b), "Continuum damage mechanics modeling of composite laminates including transverse cracks" *Int. J. Damage Mech.*, **27**(6), 877-895. https://doi.org/10.1177/1056789517711238.
Rezoug, T., Benkhedda, A., Khodjet-Kesba, M. and Adda, E.A.B. (2011), "Analysis of the composite patches cracked and aged in hygrothermal conditions", *Mech. Ind.*, **12**(5), 395-398. https://doi.org/10.1051/meca/2011134.
Shen, C.H. and Springer, G.S. (1976), "Moisture absorption and desorption of composite materials", *J. Compos. Mater.*, **10**(2), 2-20. https://doi.org/10.1177/002199837601000101.
Tamrakar, S., Couvreur, R., Mielewski, D., Gillespie Jr, J.W. and Kiziltas, A. (2023), "Effects of recycling and hygrothermal environment on mechanical properties of thermoplastic composites", *Polym. Degrad. Stabil.*, **207**, 110233. https://doi.org/10.1016/j.polymdegradstab.2022.110233.

Tounsi, A., Amara, K.H. and Adda-bedia, E. (2005), "Analysis of transverse cracking and stiffness loss in cross-ply laminates with hygrothermal conditions", *Comput. Mater. Sci*., **32**(2), 167-174. https://doi.org/10.1016/j.commatsci.2004.06.005.

Tounsi, A., Amara, K.H., Benzair, A. and Megueni, A. (2006), "On the transverse cracking and stiffness degradation of aged angle-ply laminates", *Mater. Lett*., **60**(21-22), 2561-2564. https://doi.org/10.1016/j.matlet.2006.01.037.

Tounsi, A. and Amara, K.H. (2005), "Stiffness degradation in hygrothermal aged cross-ply laminate with transverse cracks", *AIAA, Journl*. **43** (8), 1836-1843. https://doi.org/10.2514/1.3925.

Tsai, S.W. (1987), *Composites Design*, Think Composites, Dayton, Paris, Tokyo.

Vingradov, V. and Hashin, Z. (2010), "Variational analysis of cracked angle-ply laminates", *Compos. Sci. Technol*.,**70**(4), 638-646. https://doi.org/10.1016/j.compscitech.2009.12.018.

Wang, G.B., Na, J.X. and Li, X.Y. (2023a), "Effect of hygrothermal aging on the high-temperature interlaminar mechanical properties of CFRP under a complex stress state", *J. Adhes*., **99**, 752-782. https://doi.org/10.1080/00218464.2022.2048823.

Wang, P., Wu, H.L., Leung, C.K. and Li, W.W (2023b), "Hygrothermal aging effects on the diffusion-degradation process of GFRP composite: Experimental study and numerical simulation", *Constr. Build. Mater*., **379**, 131075. https://doi.org/10.1016/j.conbuildmat.2023.131075.

Xian, G., Guo, R. and Li, C. (2022a), "Combined effects of sustained bending loading, water immersion and fiber hybrid mode on the mechanical properties of carbon/glass fiber reinforced polymer composite", *Compos. Struct*., **281**, 115060. https://doi.org/10.1016/j.compstruct.2021.115060.

Xian, G., Guo, R., Li, C. and Wang, Y. (2022b), "Mechanical performance evolution and life prediction of prestressed CFRP plate exposed to hygrothermal and freeze-thaw environments", *Compos. Struct*., **293**, 115719. https://doi.org/10.1016/j.compstruct.2022.115719.

Yas, M.H., Bayat, A., Kamarian, S., Malekshahi, A. and Song, J.I. (2023), "Buckling analysis and design optimization of trapezoidal composite plates under hygrothermal environments", *Compos. Struct*., **315**, 116935. https://doi.org/10.1016/j.compstruct.2023.116935.

CC